

Multiwavelength Observations of the Black Hole Candidate XTE J1550-564 during the 2000 Outburst

Raj K. Jain^{1,2}, Charles D. Bailyn², Jerome A. Orosz³, Jeffrey E. McClintock⁴, and Ronald A. Remillard⁵

ABSTRACT

We report optical, infrared, and X-ray light curves for the outburst, in 2000, of the black hole candidate XTE J1550-564. We find that the start of the outburst in the H and V bands precedes that seen in the RXTE All Sky Monitor by 11.5 ± 0.9 and 8.8 ± 0.6 days, respectively; a similar delay has been observed in two other systems. About 50 days after the primary maxima in the VIH light curves, we find secondary maxima, most prominently in H . This secondary peak is absent in the X-ray light curve, but coincides with a transition to the low/hard state. We suggest that this secondary peak may be due to non-thermal emission associated with the formation of a jet.

Subject headings: black hole physics — X-rays: stars — stars: individual (XTE J1550-564)

1. Introduction

X-ray novae (XNe) are mass transferring binaries in which long periods of quiescence (when the X-ray luminosity is $\leq 10^{33}$ ergs s^{-1}) are occasionally interrupted by luminous X-ray and optical outbursts (Tanaka & Shibazaki 1996). XNe provide compelling evidence for the existence of stellar mass black holes (Cowley 1992; van Paradijs & McClintock 1995), since they can be shown to contain compact objects whose mass exceed the maximum stable limit of a neutron star, which is $\approx 3M_{\odot}$ (Chitre & Hartle 1976). Observations of the companion star in quiescence can lead to a full understanding of the orbital parameters of the system, including the masses of the binary components and the orbital inclination (Bailyn et al. 1998).

¹Department of Physics, Yale University, P. O. Box 208120, New Haven, CT 06520-8120, raj.jain@yale.edu

²Department of Astronomy, Yale University, P. O. Box 208101, New Haven, CT 06520-8101, bailyn@astro.yale.edu

³Sterrenkundig Instituut, Universiteit Utrecht, Postbus 80.000, 3508 TA Utrecht, The Netherlands, J.A.Orosz@astro.uu.nl

⁴Harvard-Smithsonian Center for Astrophysics, 60 Garden Street, Cambridge, MA 02138-1516, jem@cfa.harvard.edu

⁵Center for Space Research, Massachusetts Institute of Technology, Cambridge, MA 02139-4307, rr@space.mit.edu

A detailed understanding of the accretion flow in these objects is of considerable importance, since the behavior of the flow close to the event horizon may give rise to tests of general relativity in the strong field limits (McClintock 1998). During their outburst cycles, XNe generally display the complete range of spectral states, from quiescent (“off”) to “low/hard” to “high/soft” to “very high”. They therefore present unique opportunities to study all of these kinds of accretion flows in a situation in which the geometry of the binary system is well understood. Multiwavelength observations covering the entire outburst cycle are of particular importance, since the different wavelength regimes probe different aspects of the accretion flow. The RXTE satellite, with its All Sky Monitor (ASM; Levine et al. 1996) and unprecedented scheduling flexibility, has set a new standard in X-ray coverage of XNe outbursts. By contrast, optical-IR (OIR) coverage over an entire outburst is often hard to arrange from ground-based facilities. Some of the difficulties are inherent to Earth-based observing (e.g. weather and daylight) but it is also true that many facilities are scheduled in short blocks determined well in advance, which precludes following unpredictable XN outbursts which can last for several months.

The YALO Consortium (Yale, A.U.R.A., Lisbon University, and The Ohio State University) was established in part to address the latter difficulty (Bailyn et al. 2000). YALO operates the Yale 1m telescope at Cerro Tololo Interamerican Observatory. Permanently mounted on the telescope is the ANDICAM instrument, constructed at Ohio State University, which contains both a TEK 2048 \times 2048 CCD and a Rockwell 1024 \times 1024 HgCdTe IR array. The light path contains a dichroic which allows optical and near IR images to be obtained simultaneously at the same position on the sky. The telescope is scheduled as a queue designed to optimize long term monitoring and quick response to unexpected events. Thus YALO is well-suited to providing optical-infrared light curves of XNe outbursts.

We have used YALO to monitor the XN XTE J1550-564 since its discovery with the RXTE ASM on 1998 September 6 (Smith et al. 1998). Details of the initial outburst (1998-1999) have been published by Sobczak et al. (1999, 2000a, 2000b), Jain et al. (1999, 2001; hereafter Paper I and II, respectively), and Remillard et al. (1999). After a brief period of quiescence between MJD 51346 to 51600, the source returned to outburst between late March and July 2000 (Smith et al. 2000; Masetti & Soria 2000; Jain & Bailyn 2000; McCollough et al. 2000). A re-flare was also detected in the black hole candidate GRO J1655-40 (Orosz et al. 1997), a source that is similar to XTE J1550-564 with respect to its outburst light curve morphology, orbital period, and X-ray QPO behavior. Recently (2001 January) XTE 1550-564 started an unprecedented third outburst (Tomsick et al. 2001; Jain, Bailyn & Tomsick 2001). Radio observations of XTE 1550-564 during the second outburst in 2000 have been reported by Corbel et al. (2001). In this paper we report our optical and infrared light curves of that outburst — our observations provide a well-sampled light curve, which is particularly unusual in the infrared. In § 2 we discuss observations and data reductions and in § 3 compare our OIR light curves with the RXTE ASM X-ray light curve. We discuss two important features of the light curves: the different times of onset of brightening in the various bandpasses, and the presence of a secondary peak in the OIR light curve, which is most

striking in the infrared. In § 4 we list some of the questions prompted but currently unanswered by this work.

2. Observations and Data Reduction

We obtained V and H images of XTE 1550-564 every clear night between MJD 51594.28 (February 20, 2000) and 51809.00 (September 22, 2000). We also obtained I band observations during the outburst between MJD 51645.16 (April 11) and MJD 51717.14 (June 22). Exposure times were 1200s in V and 600s to 900s in I . We obtained 345 frames in V and 120 frames in I . H -band images were constructed by averaging 4 to 12 contiguous dithered frames of 80 to 95 seconds each. The dithered images were flat-field corrected, and then used to create a median sky image, which was subtracted from the individual frames before they were shifted and co-added. In this manner we constructed 425 combined H images. Typically one to four images, and at times up to eight images were obtained per filter per night.

The optical light curve was generated from differential magnitudes with respect to the four neighboring non-varying stars shown in Figure 2 of Paper II. H -band data were calibrated using standard stars reported in Persson et al. (1998). OIR light curves and RXTE ASM and hardness ratio plots are displayed in Figure 1, and prominent morphological features are indicated, when appropriate.

3. Discussion

In this paper, we will focus on two features of Figure 1, namely the delay between the start of the outburst in the OIR and in the X-ray, and the secondary peak, which is most prominent in the H-band light curve. Additional details of the light curve and its implications are discussed by Jain (2001).

3.1. Initial Rise

Figure 2 shows the start of the outburst. A linear rise is fit to the initial data in V , H , and X-ray bands. Following the procedures described by Orosz et al. (1997) for GRO J1655-40, and Jain et al. (in preparation) for Aql X-1, we define the start of the initial rise as the time when the fit to the linear portion of the earliest rise intersects the quiescent level (see Fig. 2). By this definition, the H outburst began on MJD 51623.7 ± 0.8 , relative to the quiescent brightness of $H = 16.2 \pm 0.1$ mag and the V -band outburst began on MJD 51626.4 ± 0.4 , relative to the quiescent level of $V = 21.6 \pm 0.2$ mag. The dominant error in the starting time of the outburst is the quiescent flux level, which varies intrinsically by up to ~ 0.3 magnitudes in both bands (Paper

II). The beginning of the X-ray rise was at 51635.2 ± 0.4 , implying an X-ray delay of 8.8 ± 0.6 days relative to the rise in V and 11.5 ± 0.9 days relative to the rise in H .

This source is the third XN in which an OIR outburst has been observed to precede an X-ray outburst. GRO J1655-40 (Orosz et al. 1997) and Aql X-1 (Jain et al., in preparation) have shown very similar X-ray delays; a somewhat shorter delay has also been reported for a different outburst of Aql X-1 (Shahbaz et al. 1998) based on a more sparsely sampled data set. These observed delays are difficult to explain in the context of a standard thin disk model, since any delay ought to be on the front-propagation timescale, which is of order hours. Hameury et al. (1998) proposed that a composite disk+ADAF (Advection Dominated Accretion Flow) scenario could explain the delay in GRO J1655-40, since in this case the observed delay would represent the time required for the inner edge of the disk to propagate through the ADAF cavity and reach the central source. In this case, the relevant timescale is the viscous timescale, which is on the order of days.

This explanation of the time delay receives some support from the fact that the delays seen in the three sources are all of approximately the same length, despite their differing orbital periods. Their periods vary by over a factor of three (19 hours for Aql X-1; 37 hours for XTE 1550-56; 63 hours for GRO J1655-40), and the timescale on which a disturbance would propagate from the outer parts of the disk or the secondary to the compact object might be expected to scale with the Roche-lobe radius of the primary. By contrast, if the inner edge of the accretion disk in quiescence is fixed at some specific distance from the compact object, then the time required for it to propagate inwards might plausibly be similar in all systems. Observations of more such time delays, particularly in systems which have recurrent outbursts, such as Aql X-1, will clearly be important in understanding the initial phases of XN outbursts. It will also be important to obtain a more physically motivated picture of what causes the transition from disk to ADAF flows.

3.2. The Secondary Flare

The maximum flux levels of the V and I light curves were followed initially by a period of exponential decay (see Fig. 1b,c). Similarly in the X-ray, the flux decayed exponentially while the spectra softened (see Fig. 1d,e). On the other hand, the H -band light curve decays more sharply after reaching its peak and exhibits an exponential decay only after MJD 51660 (see Fig. 1a). The e-folding time during this primary decay is progressively shorter from H to V , and is extremely short in the X-ray (see Table 1).

While the ASM light curve decays smoothly to quiescence, the VIH light curves are punctuated by a prominent secondary maximum (see Fig. 1a,b,c). During this secondary flare, the VIH light curves increased in brightness until MJD 51699 \sim 51705, after which the source brightness again decayed exponentially. Compared to the peak brightness during the initial rise, the H band secondary flare peak is only 0.52 ± 0.07 mags fainter, relative to the initial peak, while the I and V secondary flare peaks are 0.73 ± 0.03 and 0.99 ± 0.01 mags fainter, respectively, than the initial

peak values (see Fig. 2). To quantify the amplitude, timing and width of the secondary peak, we parameterize the decay light curves by fitting a Gaussian and an exponential decay to the *VIH* light curves between MJD 51658 and 51741. Although the fits are statistically poor, due to the obvious limitation of such a simple model, they are visually compelling (see Fig. 3). We find that the secondary peak is significantly sharper in *H*, compared to the peaks in *I* and *V* which occurred 3.6 ± 0.2 and 4.8 ± 0.2 days after the *H* band peak, respectively. Table 1 reports the parameters of our best fits to the Gaussian plus exponential.

In order to explain this secondary peak by X-ray reprocessing, one would have to postulate that X-rays with energies above the ASM bandpass behaved in a way that was not reflected at all in the ASM data. This objection is perhaps not insuperable given the change in X-ray hardness that occurred at about the same time, when the source entered the low/hard state (see Fig. 1e). But it appears unlikely to us that the secondary peak is reprocessed X-rays or any other thermal emission. A thermal origin for the excess flux would require a low temperature to account for the dominance of the *H*-band, and therefore a large volume to create the necessary flux. Given the 1.5 day orbital period (Paper II), such a large volume might be hard to accommodate. Exact calculations must await determinations of the geometry of the system which will be carried out when the source finally reaches quiescence. Instead, we suggest that the secondary peak may be caused by non-thermal emission, perhaps synchrotron radiation associated with a jet. Jet emission may preferentially occur when the source enters the low/hard state (Fender 2001), which occurs at $\approx 10\%$ of the Eddington limit (Esin, McClintock & Narayan 1997). This interpretation is strengthened by the $\sim 1\text{mJy}$ 8640 MHz radio detection on MJD 51697.14 (Corbel et al. 2001). Based on *V*, *I* and radio data, Corbel et al. (2001) find an inverted radio spectrum with a spectral index of 0.37 ± 0.1 , which has been interpreted as evidence for optically thick synchrotron emission arising from a compact and conical jet (Hjellming & Johnston 1988). In the future, it may be useful to use IR light curves as a trigger for extensive radio observations to determine if jets do indeed accompany such IR-dominated secondary peaks.

4. Unanswered Questions

Our work poses a number of interesting questions. Are all XN outbursts preceded by a rise in OIR flux approximately a week prior to the detection of significant X-ray flux? If so, is this timescale set by the viscous propagation time through the ADAF (§3.1)? Do secondary peaks of the kind we observed occur frequently in IR light curves of XN outbursts? Are the “plateaus” occasionally observed in optical decay light curves (e.g. see Paper II) evidence of secondary outbursts which would have been more clearly seen in the IR? Are such secondary outbursts indeed associated with jet production? Do they always coincide with a transition to a low/hard state, or to a specific flux level in the X-ray?

To answer these questions it will be necessary to carry out full multiwavelength monitoring of XN outbursts in radio, OIR and high-energy regimes. While such campaigns are hard to arrange,

the physical and astronomical importance of accretion flows onto black holes and neutron stars warrants the effort.

We thank the two YALO observers, David Gonzalez Huerta and Juan Espinoza, for providing data in a timely manner. We would like to thank S. Tourtellotte and E. Terry for their assistance with data reduction and J. Yong, R. Winnick, & B. Roscherr for their assistance with computer facilities as well as useful discussions. We would like to thank S. Corbel for discussions on radio data and M. Nowak, T. Maccarone, and P. Coppi for extensive discussions on the interpretations of the light curves. Financial support for this work was provided by the National Science Foundation through grant AST 97-30774.

REFERENCES

- Bailyn, C. D., Depoy, D., Agostinho, R., Mendez, R., Espinoza, J., & Gonzalez, D. 2000, AAS, 195.8706B
- Bailyn, C. D., Jain, R. K., Coppi, P., & Orosz, J. A. 1998, ApJ, 499, 367
- Chitre, D. M., & Hartle, J. B. 1976, ApJ, 207, 592
- Corbel, S., et al. 2001, ApJ, in press (astro-ph/0102114)
- Cowley, A. P. 1992, ARA&A, 30, 287
- Esin, A. A., McClintock, J. E., & Narayan, R. 1997, ApJ, 489, 865
- Fender, R. P. 2001, MNRAS, 322, 31
- Hameury, J.-M., Lastoa, J.-P., McClintock, J. E., & Narayan, R. 1997, ApJ, 489, 234
- Hjellming, R. M., & Johnston, K. J. 1988, ApJ, 328, 600
- Jain R. K. 2001, Ph.D. Thesis, Yale University
- Jain, R. K., & Bailyn, C. D. 2000, IAU Circ. 7400
- Jain, R. K., Bailyn, C. D., Orosz, J. A., Remillard, R.A., & McClintock, J. E. 1999, ApJ, 517, L131 (Paper I)
- Jain, R., Bailyn, C. D., Orosz, J. A., McClintock, J. E., Sobczak, G. J., & Remillard, R.A. 2001, ApJ, 546, 1086 (Paper II)
- Jain, R., Bailyn, C., & Tomsick, J. 2001, IAU Circ. 7575
- Levine, A. M. et al. 1996, ApJ, 469, L33

- Masetti, N., & Soria, R. 2000, IAU Circ. 7399
- McClintock, J. E. 1998, in AIP Conf. Proc. 431, *Accretion Processes in Astrophysics: Some Like it Hot*, ed. S. Holt & T. Kallman (Woodbury, NY: AIP), 290
- McCullough, M. L., Wilson, C. A., & X. Sun 2000, IAU Circ. 7400
- Orosz, J. A., Remillard, R. A., Bailyn, C. D., & McClintock, J. E. 1997, ApJ, 478, L83
- Persson, S. E., Murphy, D. C., Krzeminsky, W., Roth, M., & Rieke, M. J. 1998, AJ, 116, 2475
- Remillard, R. A., McClintock, J. E., Sobczak, G. J., Bailyn, C. D., Orosz, J. A., Morgan, E. H., & Levine, A. M. 1999, ApJ, 517, L127
- Shahbaz, T., Bandyopadhyay, R. M., Charles, P. A., Wagner, R. M., Muhli, P., Hakala, P., Casares, J., & Greenhill, J. 1998, MNRAS, 300, 1035
- Smith, D. A., Levine, A. M., Remillard, R., & Fox, D. 2000, IAU Circ. 7399
- Sobczak, G. J., McClintock, J. E., Remillard, R. A., Levine, A. M., Morgan, E. H., Bailyn, C. D., & Orosz, J. A. 1999 ApJ, 517, L121
- Sobczak, G. J., McClintock, J. E., Remillard, R. A., Cui, W., Levine, A. M., Morgan, E. H., Orosz, J. A. & Bailyn, C. D. 2000a, ApJ, 531, 537
- Sobczak, G. J., McClintock, J. E., Remillard, R. A., Cui, W., Levine, A. M., Morgan, E. H., Orosz, J. A. & Bailyn, C. D. 2000b, ApJ, 544, 993
- Tanaka, Y. & Shibazaki, N. 1996, ARA&A, 34, 607
- Tomsick, J. A., Smith, E., Swank, J., Wijnands, R., & Homan, J. 2001, IAU Circ. 7575
- van Paradijs, J., & McClintock, J. E. 1995 in “X-ray Binaries”, eds. W. H. G. Lewin, J. van Paradijs, & E. P. J. van den Heuvel, Cambridge University Press, Cambridge, England, page 58

Table 1. Summary of Optical and X-ray Light Curves

Filter	Initial Rise			Primary Decay		Secondary Flare		
	Start (MJD-51000)	Slope (mag/d)	Peak (MJD-51000,mag)	Dates (MJD-51000)	τ_e (d)	Dates (MJD-51000)	Peak ^b (MJD-51000)	FWHM ^b (d)
<i>H</i>	623.7 ± 0.8	-0.132 ± 0.003	654.3, 13.36 ± 0.05	654.2~688	46.2 ± 1.4^a	688~747.2	700.7 ± 0.1	16.7 ± 0.2
<i>I</i>	653.4, 15.92 ± 0.02	653.4~688	33.6 ± 0.3^c	...	704.3 ± 0.2	21.5 ± 0.4
<i>V</i>	626.4 ± 0.4	-0.511 ± 0.009	653.4, 17.89 ± 0.02	653.4 ~ 688	30.4 ± 0.3^d	688 ~ 750.9	705.5 ± 0.2	19.4 ± 0.4
ASM	635.2 ± 0.4	0.0142 ± 0.001^e	661.8, 0.99 ± 0.02^f	661.8 ~ 701	10.8 ± 0.2^g

^aFit to MJD 51660-51686

^bDetermined by a Gaussian+linear fit to data between MJD 51658-51741

^cFit to MJD 51655-51686

^dFit to MJD 51655-51686

^eCrabs day⁻¹

^fCrabs

^gFit to MJD 51661~51680

Figure Legends

Fig. 1.— From top to bottom: YALO H , I , V , RXTE/ASM, and ASM HR2 = (5-12 keV/3-5 keV) light curves. The distinctive morphological features, when appropriate, are denoted by the vertical lines, where I. R., P. D., and S. F., denote the initial rise, primary decay and secondary flare, respectively (see Table 1 for exact dates and corresponding light curve properties). Note the prominent secondary flare, which is absent in the X-rays, but coincides with a state transition apparent in the hardness ratio curve.

Fig. 2.— Top to bottom: The H , V , and RXTE/ASM light curves during the initial rise. A linear fit was made to the data between MJD 51625–51635, MJD 51626–51631, and MJD 51635–51644 in H , V , and ASM, respectively. Based on these fits the start of the X-ray rise is delayed by of 8.8 ± 0.6 and 11.5 ± 0.9 days relative to the V and H band, respectively.

Fig. 3.— Top to Bottom: A Gaussian plus linear fit to the VIH data during the secondary flare (see Table 1). quantifying the width and peak of the flare. The best fit values to the times, size, and width of the Gaussians are recorded in Table 1. The secondary peak is significantly sharper in H , compared to those of I and V which occurred several days after the H band peak.

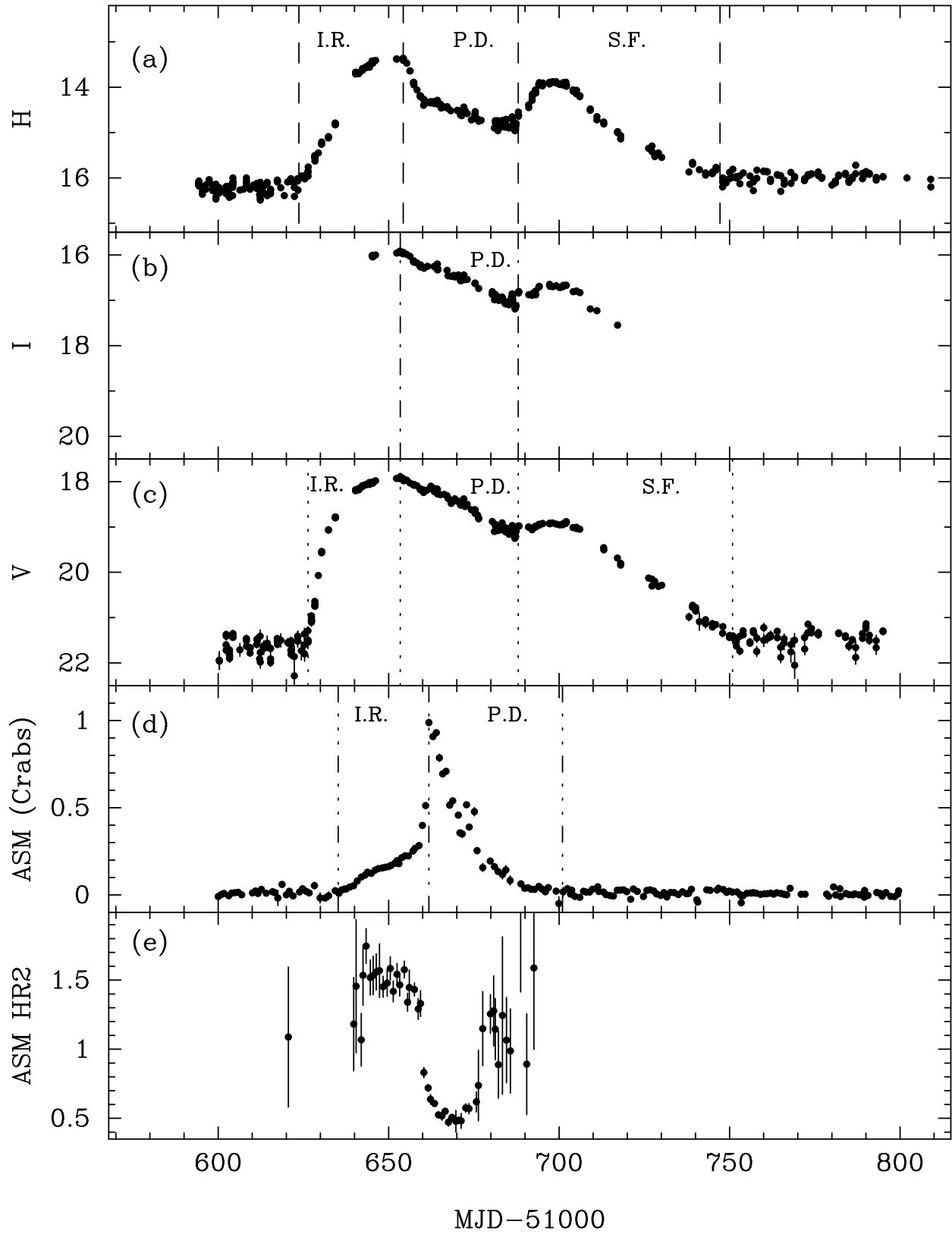


Fig. 1.—

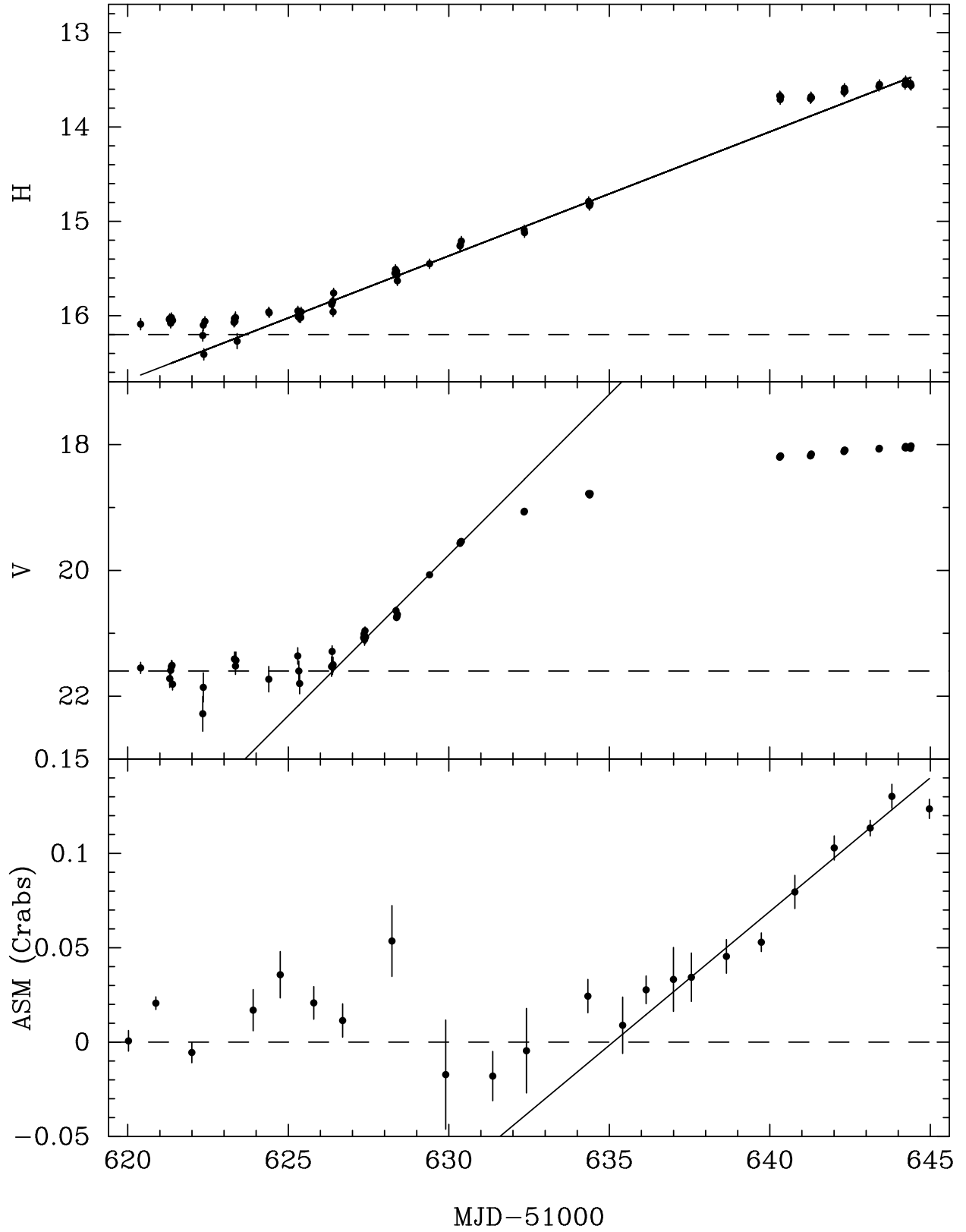


Fig. 2.—

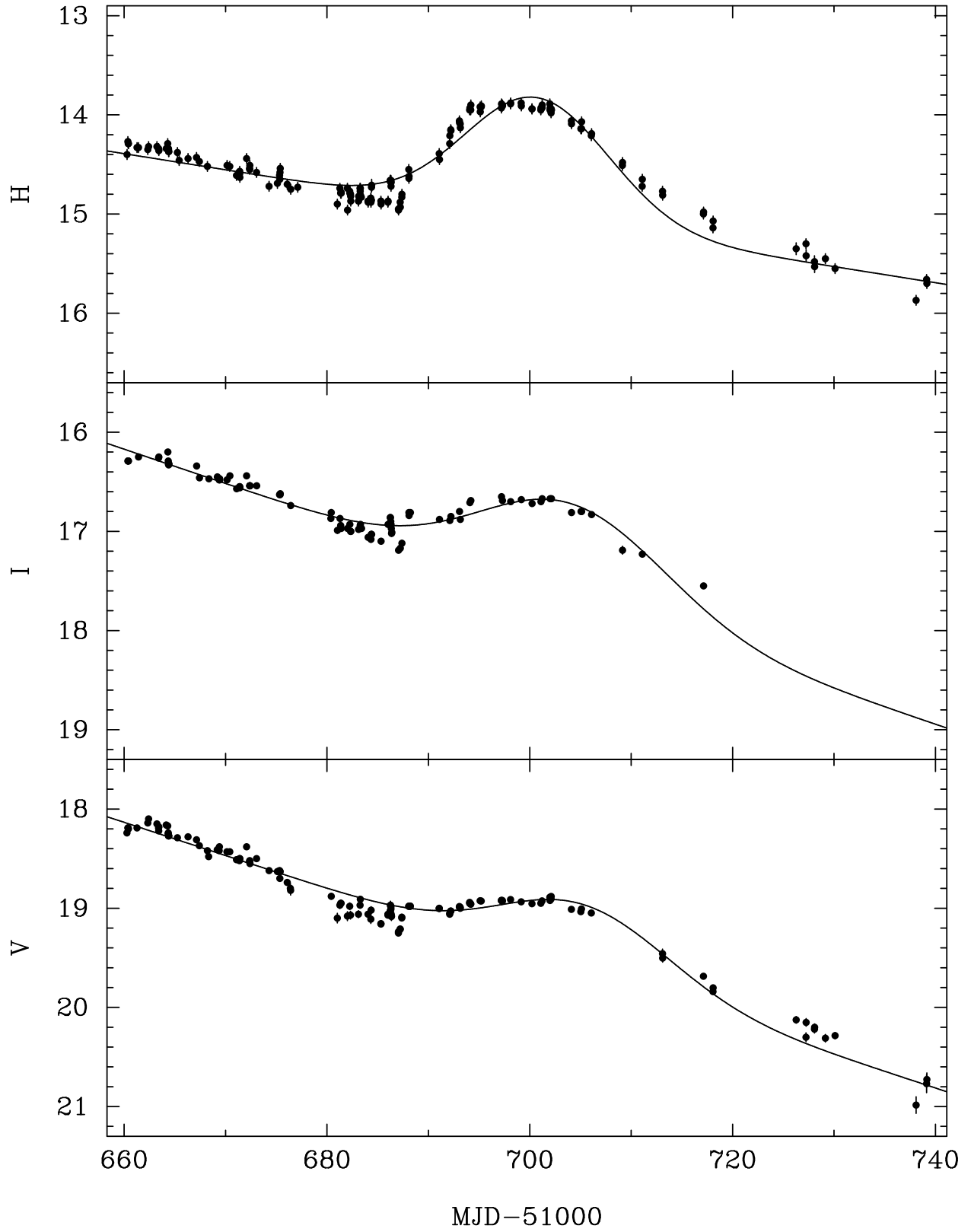


Fig. 3.—